Environmental Pollution 267 (2020) 115616

Contents lists available at ScienceDirect

Environmental Pollution

journal homepage: www.elsevier.com/locate/envpol

Using Zn isotopes to trace Zn sources and migration pathways in paddy soils around mining area☆

Yuhui Liu [a, b, 1], Ting Gao [a, b, c, 1], Yafei Xia [a, b], Zhengrong Wang [d], Chengshuai Liu [a, c, *], Shehong Li [a], Qiqi Wu [c], Meng Qi [a, b], Yiwen Lv [c]

[a] State Key Laboratory of Environmental Geochemistry, Institute of Geochemistry, Chinese Academy of Sciences, Guiyang, 550081, PR China
[b] University of Chinese Academy of Sciences, Beijing, 100049, PR China
[c] National-Regional Joint Engineering Research Center for Soil Pollution Control and Remediation in South China, Guangdong Key Laboratory of Integrated Agro-environmental Pollution Control and Management, Guangdong Institute of Eco-environmental Science & Technology, Guangdong Academy of Sciences, Guangzhou, 510650, PR China
[d] Department of Earth & Atmospheric Sciences, The City College of New York, CUNY, New York, 10031, USA

ARTICLE INFO

Article history:
Received 25 April 2020
Received in revised form
19 August 2020
Accepted 5 September 2020
Available online 8 September 2020

Keywords:
Heavy metal pollution
Zn isotopes
Migration processes
Fe-bearing minerals
Paddy soil

ABSTRACT

Paddy soils around mining areas suffer from the great threat of heavy metal pollution. The traditional source-tracing methods based on metal concentrations limit our ability to quantify the sources of heavy metals and trace their transport processes to paddy soils. In this study, Zn isotope compositions of paddy soils in Dabaoshan mine area, a typical sulfide deposit in southern China, have been systematically studied. According to a plot between 1/Zn (i.e. inverse concentration) and δ^{66}Zn value, all the polluted paddy soils fall on the mixing line between acid mine drainage precipitate (AMD-precipitate) and fertilizer while the unpolluted paddy soil falls on the mixing line between fertilizer and bedrock. This indicates the mixing of Zn sources at least three end-members: the mining end-member (i.e. AMD-precipitate), the agricultural end-member (i.e. fertilizer), and bedrock whose geochemical signature is often overprinted by the former two sources around the mining area. The quantitative calculations to apportion the end-member's contributions show that the mining activity contributes most Zn in the paddy soils with an average of ~66.2%. The contribution of mining activities has significant spatial variations. Specifically, the mining activities have relatively low impacts on the lower reach and the deep soil. Additionally, the apparent Zn isotope fractionation between AMD and AMD-precipitate ($\Delta^{66}Zn_{AMD\text{-}precipitate\ -\ AMD}$ of −0.35 to −0.08‰) in the tailings dam suggests that Zn cations in AMD coprecipitated with the secondary Fe-bearing minerals (e.g. jarosite and goethite). After being discharged from the tailings dam, Zn is mainly carried by the Fe-oxide minerals and migrated during surface runoff. Our study highlights the contribution of human activities to the Zn pollution in the paddy soils and the key role of Fe-bearing minerals in the migration of Zn. These findings provide a scientific base for the development of policy for pollution control in mining-affected region.

1. Introduction

The metal mining activities usually produce wastes including acid mine drainages (AMD), mine tailings, and fly ashes, which contain high concentrations of heavy metals (Mattielli et al., 2009; Dold, 2014; Qu et al., 2017; Chen et al., 2018; Roebbert et al., 2018; Liu et al., 2019). Soil is a long-term sink for heavy metals (Wuana and Okieimen, 2011; Chen et al., 2018) and heavy metals from these wastes can be transported from mining areas to the surrounding soils through surface runoff and/or dust particles (Mattielli et al., 2009; Dold, 2014; Yang et al., 2019). As a result, mining has been considered as one of the most significant sources of heavy metal pollution for agricultural soils (Liu et al., 2005; Acosta et al., 2011; Li et al., 2014; Wen et al., 2015).

Identifying the sources of pollution is the first and critical step for mitigating the heavy metal contamination in soils (e.g. Zhao

☆ This paper has been recommended for acceptance by Philip N. Smith.
* Corresponding authors. State Key Laboratory of Environmental Geochemistry, Institute of Geochemistry, Chinese Academy of Sciences, Guiyang, 550081, PR China.
E-mail address: liuchengshuai@vip.gyig.ac.cn (C. Liu).
[1] These authors contributed equally to this work.

https://doi.org/10.1016/j.envpol.2020.115616
0269-7491/

et al., 2015; Kumar et al., 2020). The traditional methods for doing so are generally based on statistical analyses of metal concentrations (e.g. Cheng and Hu, 2010). However, they are limited in tracing pollution origins in complex environments due to the multiple sources involved and the large number of samples needed (Wen et al., 2015; Sherman et al., 2015). In recent years, with the development of isotope analytic technique, the metal stable isotopes have been shown to serve as powerful tools to trace the sources and biogeochemical processes of heavy metals in environments (Kumar et al., 2009; Juillot et al., 2011; Wiederhold, 2015; Schudel et al., 2018; Li et al., 2019).

As one of the effective geochemical indicator elements in exploration, zinc (Zn) involves in a number of biogeochemical processes in atmosphere (Mattielli et al., 2009), soil (Imseng et al., 2019), and river (Zimmermann et al., 2020). Previous studies have indicated that Zn isotope signature can be used to trace biogeochemical processes (e.g. Wiederhold, 2015; Moynier et al., 2017) since characteristic Zn isotope fractionations occur during many environmental processes, including inorganic precipitation (Mavromatis et al., 2019), evaporation (Zhang and Liu, 2018; Wimpenny et al., 2019), organic complexation (Jouvin et al., 2009), sorption to minerals (Pokrovsky et al., 2005; Juillot et al., 2008; Bryan et al., 2015; Guinoiseau et al., 2016; Gou et al., 2018), and biological uptake (Weiss et al., 2005; Arnold et al., 2010; Wiggenhauser et al., 2018). Moreover, the Zn isotope compositions of anthropogenic materials are significantly different from those in natural reactions (Mattielli et al., 2009; Juillot et al., 2011; Fekiacova et al., 2015; Li et al., 2019). For example, high-temperature processes during metallurgical processing can lead a large Zn isotope fractionation in slag and vapor phase (Juillot et al., 2011; Shiel et al., 2010; Mattielli et al., 2009), but the fractionation caused by high-temperature magmatic process is small (Chen et al., 2013). Therefore, Zn isotopes have been used to identify the contribution of anthropogenic Zn pollution to river water (Chen et al., 2008), suspended particulate matters (Chen et al., 2009), and soils (Bigalke et al., 2010; Juillot et al., 2011; Fekiacova et al., 2015; Imseng et al., 2019; Xia et al., 2020).

Most previous studies on Zn isotopes in soils have mainly focused on smelter-affected (Bigalke et al., 2010; Juillot et al., 2011) or agricultural region (Fekiacova et al., 2015; Imseng et al., 2019), and have successfully identified the Zn sources in soils. However, only a few studies have reported the specific migration pathways of Zn and quantified the contributions of the different Zn sources to soils (e.g. Xia et al., 2020).

In this study, we systematically investigated the Zn isotope compositions of paddy soil, river sediment, acid mine drainage precipitate (AMD-precipitate), ore, fertilizer, rice plant, bedrock, dry deposition, rainwater, river water, and AMD samples around the Dabaoshan mine, Guangdong Province, southern China. Our work aims to quantify the contributions of the specific Zn pollution sources to paddy soils and reveal the Zn migration pathways in a mining area. The findings are expected to provide a scientific base for the development of technology and policy for pollution control in the mining-affected region.

2. Study site, sample collection and pretreatment

The study area is around the Dabaoshan mine in Guangdong Province, southern China (113°43′13″E, 24°31′36″N; Fig. 1). This region is characterized by a subtropical monsoon climate with a mean annual temperature of ~20 °C and mean annual rainfall of ~1550 mm, and subtropical red soil. Dabaoshan mine is a large-scale polymetallic sulfide deposit which has been mined for more than forty years. The main ore minerals of the deposit include pyrite, chalcopyrite, pyrrhotite, sphalerite, and galena (Ye et al., 2014). During mining activities, a large quantity of mine wastes has been discharged into the Hengshi (HS) River, a river originating from the mine area (Zhou et al., 2007).

A total of 7 topsoil samples (approximately 0–5 cm in depth), 4 sediment samples, and 7 river water samples were collected from the upper (sites 5–9,11) and lower reach (sites 12–14) of the HS river irrigation area (Fig. 1). As a comparison, a topsoil (TS-0), a river sediment (TC-0), and a river water sample (TW-0) were collected from a site (site 10) located beside the Taiping (TP) river irrigation area which is a non-contaminated tributary of the HS river. Two paddy soil profiles, Tangxin (TX) and Shengli (SL), were sampled at sites 8 and 14, respectively. Four horizons were identified along each soil profile based on the color, particle size, and moisture, including plow horizon (A), plow horizon (P), waterloggogenic horizon (W), and parent material horizon (C) (Gao et al., 2018). The samples of ore, AMD, and AMD-precipitate were collected from three sampling sites (sites 1–3) in the Liwu tailings dam. Additionally, two bedrocks, a fertilizer, three dry depositions, and two rainwater samples were collected at site 11, which is located at the midpoint of the studied section of the HS river. Two rice plant samples, rice 1 and rice 2, were gathered from TX profile and SL profile, respectively. Water samples were collected with acid-cleaned polypropylene (PP) bottles. Dry deposition samples were collected with polyvinyl chloride (PVC) plates with Whatman®41 cellulose filters following the method reported by Mattielli et al. (2009). All samples were collected in October 2017 and July 2020 during the harvest season of rice.

The samples of paddy soil, river sediment, and AMD-precipitate were air-dried at room temperature, followed by the removal of biological debris. The solid samples were ground into fine powder and passed through a 200-mesh nylon sieve. The water samples were filtered with 0.22-μm cellulose acetate filters, and then acidified to pH < 2 with ultrapure HNO_3. Water samples after filtration were stored in a refrigerator at ~4 °C before analysis. Rice plants were washed with deionized water and separated into root, grain, and straw. After being dried in an oven at ~105 °C for ~1.5 h and then ~75 °C for ~48 h, all of these rice samples were ground into fine powder.

3. Materials and methods

3.1. Analyses of TOC, pH, and metal concentrations

The pH values of paddy soils, sediments, and AMD-precipitates were measured using a pH meter (PB-10, Sartorius, Germany) after equilibrating ~5 g of solid powder and ~12.5 mL of deionized water for ~2 h. The total organic carbon (TOC) content was determined on a CHNS analyzer (vario MACRO cube, Elementar Analysensysteme GmbH, Germany). Measurements of major (Al and Fe) and trace (Zn) elements were performed on an inductively coupled plasma optical emission spectroscopy (ICP-OES, Optima 8000, PerkinElmer, USA) and an inductively coupled plasma mass spectrometry (ICP-MS, NexION 300X, PerkinElmer, USA), respectively. Prior to measurements, ~0.04 g of each solid sample was completely digested in ~3.5 mL of a 1:1:3 (v/v) mixture of HF–HCl–HNO_3 and ~100 mL of each liquid sample was dried on hot plate. The samples were re-dissolved in ~3% HNO_3 for major and trace element analyses. The instrument drift was calibrated by the internal standard of Rh. United States Geological Survey (USGS) reference material of BHVO-2 was used for quality control of the analysis. Detection limits for Fe and Al analyzed by ICP-OES are 5 and 20 μg L^{-1},

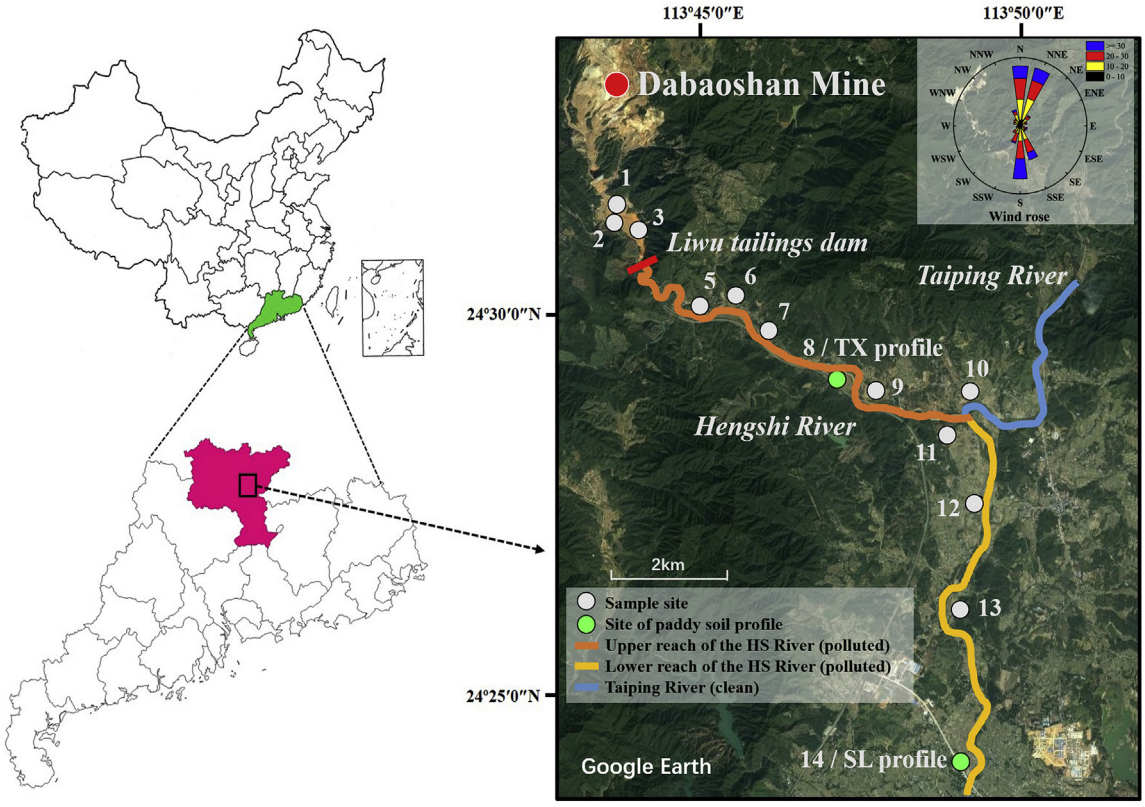

Fig. 1. Map showing the Dabaoshan mine and the location of sample sites along the HS and TP river. Two paddy soil profiles were set at site 8 and 14.

respectively, and detection limit for Zn analyzed by ICP-MS is 0.001 μg L^{-1}. The relative standard deviations (RSD) of our measurements are better than 2% for major element analyses and 10% for Zn concentration measurements.

3.2. Characterization of mineral phase

The mineral modes of paddy soils, sediments, and AMD-precipitates were characterized by an X-ray powder diffractometer (XRD, Bruker D2, Germany). The Co/Kα radiation was used for generating X-rays, which was scanned over 5–85° at a speed of ~1.2°/min with a step size of ~0.02°. The TOPAS V5 software (Bruker AXS, Germany) was used to quantify the mineral mode using the Rietveld method (Young, 1993; Perl et al., 2012).

3.3. Selective sequential extraction experiments

To investigate the Zn speciation in paddy soils and sediments, the selective sequential extraction method, modified after Yin et al. (2016), was employed to separate Zn of different forms. This method can effectively extract heavy metals bound to well-crystallized iron (hydro)oxides. Zinc in soils was separated into the following fractions: the exchangeable fraction (F1), the carbonate associated fraction (F2), the easily reducible Fe–Mn oxide associated fraction (F3), the organic associated fraction (F4), the well crystallized iron oxide associated fraction (F5), and the residual fraction (F6). The details of the sequential extraction procedure are provided in Table S1. Each supernatant solution was separated from the insoluble residue by a centrifuge at ~9168×*g* for 30 min. Zinc concentrations of all supernatant solutions were measured using ICP-MS.

3.4. Zinc isotope analyses

3.4.1. Sample digestion and Zn purification

All sample digestion and Zn purification procedures were performed in class-100 laminar flow hoods of a class-1000 clean-room at Guangdong Institute of Eco-environmental Science & Technology, Guangzhou, China. All acid reagents (including HF, HCl, and HNO_3) were distilled on the acid purification system (DST-1000, Savillex, USA). Trace elemental analysis grade H_2O_2 (Fisher chemical, USA) and ultra-pure Milli-Q water (18.2 MΩ cm) were used during the Zn purification.

Depending on the Zn concentration, a certain amount of each sample was weighted to ensure ~2 μg of Zn after digestion. Approximately 10–400 mg of solid samples (except for vegetation samples) and USGS reference materials of BHVO-2, GSP-2, and NOD-A-1 were weighted into Perfluoroalkoxy alkanes (PFA) beakers (Savillex, USA). About 3.2 mL of concentrated HF–HNO_3 mixture (3:1, v/v) was added to each beaker, which was then heated on a hot plate at ~150 °C overnight. After being cooled in air, each sample was evaporated to dryness at ~160 °C. Afterwards, about 4 mL of aqua regia was added into the beakers, followed by heating at ~140 °C for 1–2 days and dried at ~80 °C. Vegetation samples were digested with ~10 mL of concentrated HF–HNO_3 mixture (1:3, v/v) at ~200 °C in a microwave oven (Ethos UP, Milestone, Italy). The supernatant solutions were transferred to PFA beakers and evaporated to dryness at ~160 °C. Subsequently, the dried samples were treated by ~4 mL of aqua regia and dried again.

About 1–250 mL of the liquid sample was dried at ~100 °C in a PFA beaker, depending again on its Zn concentration. Then, about 2 mL of aqua regia was added, followed by heating at ~140 °C for 1–2 days and drying at ~80 °C. All dried samples were then re-dissolved in ~1 mL of concentrated HCl and heated to dryness

again. The dried samples were finally dissolved in ~1 mL of 8 N HCl + 0.001% H_2O_2 for chromatographic separation.

The dissolved Zn was purified by anion-exchange chromatography with ~2 mL of AG-MP-1M resin (Bio-Rad 100–200 mesh) following the protocol by Lv et al. (2016). Matrix components were removed with ~10 mL of 8 N HCl + 0.001% H_2O_2. Then, ~24 mL of 8 N HCl + 0.001% H_2O_2 and ~18 mL of 2 N HCl + 0.001% H_2O_2 were added to elute Cu and Fe, respectively. Zinc was collected using ~10 mL of 0.5 N HNO_3 after ~2 mL of 0.5 N HNO_3 was discarded.

3.4.2. Mass spectrometry

Zinc isotope ratio measurements were carried out on a MC-ICP-MS (Neptune Plus, Thermo Fisher, USA) in wet plasma mode at State Key Laboratory of Environmental Geochemistry, Institute of Geochemistry, Chinese Academy of Sciences. The sample-standard bracketing (SSB) method was employed to correct instrumental mass bias. All samples and standards (IRMM 3702) were diluted to ~200 ppb in 3% HNO_3 prior to analysis. Measurements were performed in low resolution mode with high-sensitivity (X) cone to ensure the ^{64}Zn signals were > 3 V/200 ppb. Each measurement was operated for 3 blocks of 30 cycles. The standard-sample sequence was repeated at least three times for each sample to achieve better reproducibility.

3.4.3. Notation

The Zn isotope compositions of all samples were expressed as $\delta^{66}Zn$ (‰) relative to the reference material IRMM 3702 according to the following equation:

$$\delta^{66}Zn\ (‰) = \left[\frac{\left(^{66}Zn/^{64}Zn\right)_{sample}}{\left(^{66}Zn/^{64}Zn\right)_{IRMM\ 3702}} - 1\right] \times 1000 \quad (1)$$

where $(^{66}Zn/^{64}Zn)_{sample}$ and $(^{66}Zn/^{64}Zn)_{IRMM\ 3702}$ refer to the ratio of ^{66}Zn and ^{64}Zn of samples and the reference material, respectively.

3.4.4. Quality assurance

The total procedural blanks are neglected and within ~6 ng for Zn. The two standard deviations (2SD) of the Zn isotope compositions for all the samples are less than 0.07 based on the repeat analyses. Geological reference materials BHVO-2, GSP-2, and NOD-A-1 yield average $\delta^{66}Zn$ values of 0.08 ± 0.02‰, 0.85 ± 0.03‰, and 0.72 ± 0.04‰, respectively, which consist with those reported previously (Chen et al., 2016; Lv et al., 2016; Moeller et al., 2012).

4. Results

4.1. Zinc concentrations

Along the HS river, the topsoils from the upper reach (DS-6, 8, 9, and 11) have an average Zn concentration of ~430 mg kg^{-1}, which is higher than that of the topsoils from the lower reach (DS-12, 13, and 14, average concentration of ~180 mg kg^{-1}). The topsoil sample from the TP river irrigation area, TS-0, has a lower Zn concentration than that from the HS river, with a value of ~59 mg kg^{-1} (Table 1). The TX profile, which is located at the upper reach of the HS river irrigation area, has an average Zn concentration of ~270 mg kg^{-1}. The downstream SL profile has lower Zn concentrations, with an average value of ~180 mg kg^{-1}. In each soil profile, the Zn concentrations of the surface horizons are the highest (Table 1).

To evaluate the pollution level of Zn in the paddy soils, the Al-normalized Zn enrichment factors (EF_{Zn}), which can cancel the dilution effect on Zn concentrations caused by natural composites, were calculated based on the following equation:

$$EF_{Zn} = \frac{(C_{Zn}/C_{Al})_{sample}}{(C_{Zn}/C_{Al})_{background}} \quad (2)$$

where C_{Zn} and C_{Al} refer to concentrations of Zn and Al, respectively. Here, the element concentration of background is based on China Environmental Monitoring Station (1990). The paddy topsoils from the upper reach of the HS river irrigation area have an average EF_{Zn} value of ~6.5, which is higher than that from the lower reach (average value of ~4.0). The topsoil from the TP river irrigation area (TS-0) shows a minimal pollution with the EF_{Zn} value of ~1.1, which is lower than any other soil samples (Table 1). The average EF_{Zn} value of TX profile is higher than that of SL profile, with an average value of ~6.2 and ~4.0, respectively (Table 1).

The river sediments, AMD-precipitates and sulfide ores have average Zn concentrations of ~2200 mg kg^{-1}, ~850 mg kg^{-1}, and ~570 mg kg^{-1}, respectively, which are higher than those in the paddy topsoils (average value of ~290 mg kg^{-1}). The average Zn concentrations of the bedrocks (~13 mg kg^{-1}), dry depositions (~180 mg kg^{-1}), and fertilizer (~150 mg kg^{-1}) are lower than those in the paddy topsoils (Table 2). The Zn concentrations of HS river water decrease with increasing distance from the Liwu tailings dam, with an average concentration of ~1.1 mg L^{-1}, which is much lower than that in the AMD (average concentration of ~120 mg L^{-1}).

4.2. Zinc isotope compositions

The $\delta^{66}Zn$ values of topsoils from the upper reach (DS-6, 8, 9, and 11) have a limited range (from −0.26 to −0.22‰). The topsoils from the lower reach (DS-12, 13, and 14) have slightly higher $\delta^{66}Zn$ values ranging from −0.17 to −0.09‰. The topsoil from the uncontaminated TP river irrigation area has the highest $\delta^{66}Zn$ values among all topsoil samples, with a $\delta^{66}Zn$ value of 0.03 ± 0.07‰ (Table 1). The Zn isotope compositions of TX profile and SL profile are also provided in Table 1. The $\delta^{66}Zn$ values of the TX profile range from −0.27 to −0.18‰, which are lower than those of the SL profile (ranging from −0.13 to 0.04‰).

In the mining area, the $\delta^{66}Zn$ values of sulfide ore (average value of 0.10 ± 0.09‰, 2SD, $n = 3$) are higher than those of AMD (average value of 0.00 ± 0.06‰, 2SD, $n = 4$) and AMD-precipitates (average value of −0.23 ± 0.15‰, 2SD, $n = 6$). The $\delta^{66}Zn$ values of bedrock (average value of 0.00 ± 0.02‰, 2SD, $n = 2$) are similar to those of bulk silicate Earth (BSE, −0.02 ± 0.05‰) (Chen et al., 2013). Both rainwater and dry deposition have negative $\delta^{66}Zn$ values of −0.14 to −0.07‰ and −0.26 to −0.18‰, respectively (Fig. 2). The $\delta^{66}Zn$ value of compound fertilizer is 0.11 ± 0.05‰ (Table 2).

The $\delta^{66}Zn$ values of different organs in rice plants present an obvious difference (Fig. 3). They are more negative in the grains (−0.65 to −0.54‰) and straws (−0.37 to −0.21‰), while the roots are generally enriched in ^{66}Zn, compared with the grains, straws, and paddy soils, with an average $\delta^{66}Zn$ value of 0.05 ± 0.08‰ (2SD, $n = 2$). Based on mass-balance, the $\delta^{66}Zn$ values of bulk rice plants can be calculated as follows:

$$\delta^{66}Zn = \frac{\sum \delta^{66}Zn_{organ} \times [Zn]_{organ} \times f_{organ}}{\sum [Zn]_{organ} \times f_{organ}} \quad (3)$$

where $[Zn]_{organ}$ and $\delta^{66}Zn_{organ}$ are Zn concentration and $\delta^{66}Zn$ value of each organ, respectively, and f_{organ} is fraction of Zn in the organ relative to the whole plant. The calculation results show that the $\delta^{66}Zn$ values of the bulk rice plants range from −0.24 to −0.17‰ (Table S2).

The $\delta^{66}Zn$ values of river water samples from the upper reach of the HS river (DW-5 to DW-8, and DW-11) vary from −0.03 to 0.15‰

Table 1
Zn isotope compositions, metal concentrations and other relevant parameters in the paddy soils.

Site	Sample	δ^{66}Zn (‰)	2SD[a]	pH	TOC (g kg^{-1})	Al (g kg^{-1})	Fe (g kg^{-1})	Zn (mg kg^{-1})	EF^{b}_{Zn}
HS river irrigation area topsoil									
6	DS-6	−0.22	0.03	5.58	13.6	59	39.9	220	4.5
8	DS-8	−0.23	0.01	5.87	11.1	53	82	280	6.3
9	DS-9	−0.24	0.03	6.09	21.8	74	79	371	5.9
11	DS-11	−0.26	0.00	6.28	17.7	109	126	833	9.1
12	DS-12	−0.09	0.05	6.20	6.52	44.9	20.6	152	4.0
13	DS-13	−0.11	0.00	6.14	22.7	62	19.6	103	2.0
14	DS-14	−0.17	0.02	6.51	10.2	56	27.2	277	5.9
TP river irrigation area topsoil									
10	TS-0	0.03	0.07	6.49	–	62	24.3	59	1.1
Horizon	Depth (cm)	Sample	δ^{66}Zn (‰)	2SD[a]	pH	TOC (g kg^{-1})	Al (g kg^{-1})	Fe (g kg^{-1})	Zn (mg kg^{-1})	EF^{b}_{Zn}
TX profile										
A	0–14	P1-A	−0.27	0.02	5.53	13.0	57	93	332	6.9
P	14–24	P1–P	−0.27	0.06	6.15	10.5	56	95	330	7.0
W	24–44	P1–W	−0.20	0.04	6.13	3.24	42.8	82	196	5.4
C	44–65	P1–C	−0.18	0.08	6.37	3.45	44.3	53	205	5.5
SL profile										
A	0–20	P2-A	−0.13	0.04	5.95	8.18	55	27.4	308	6.7
P	20–38	P2–P	0.04	0.07	6.54	4.18	56	27.3	128	2.7
W	38–63	P2–W	−0.01	0.03	7.12	2.61	53	31.6	142	3.2
C	63–80	P2–C	0.02	0.03	6.62	1.73	46.3	23.1	126	3.2

[a] 2 times the standard deviation of δ^{66}Zn was calculated from the replicates of each sample.
[b] Enrichment factor of Zn (EF_{Zn}) was calculated based on equation (2).

and increase with increasing distance from the Liwu tailing dam. The river water samples from the lower reach of the HS river (DW-12 and DW-14) have δ^{66}Zn values ranging from 0.08 to 0.28‰, which are slightly higher than those from the upper reach (Table 2). All δ^{66}Zn values of river water samples are higher than those of the paddy soils (Fig. 2). Fluctuated along the HS river, the δ^{66}Zn values of sediments in HS river range from −0.12 to −0.03‰.

4.3. Mineral mode

The mineral modes of paddy soils, AMD-precipitates, sediments, and ores are presented in Table S3. The paddy topsoils mainly consist of quartz, muscovite, goethite, kaolinite, phengite, and microcline, with mean percentages of ~52.1%, ~16.1%, ~8.4%, ~5.5%, ~12.7%, and ~5.3%, respectively. The goethite contents in topsoil samples obtain maximal values at surface horizon and gradually decrease downward along each profile. The only kind of clay minerals in the studied paddy soils is kaolinite. Pyrite and chalcopyrite are the main ore minerals in the ore samples. Various sulfide minerals and secondary Fe-oxide minerals appear in the AMD-precipitates, which included goethite, jarosite and hematite. The bedrock is sandstone, which mainly consists of quartz and muscovite.

4.4. The fractions of Zn in paddy soils

Fig. S1 illustrates the Zn fractions of different supernatants relative to bulk samples from our selective sequential extraction experiments. The Zn fractions associated with easily-reducible Fe–Mn oxides (40.1–62.1%) and the well-crystallized iron oxides (3.8–21.4%), and in the residuals (9.3–36.5%) are the three main phases of Zn in paddy soils (including topsoils and soils in the profile). The Zn proportions of the exchangeable fraction (1.8–14.6%), carbonate associated fraction (0.4–4.6%), and organic associated fraction (5.1–10.0%) are relatively low. In addition, the Zn fractions associated with the total Fe–Mn oxides (including both reducible Fe–Mn oxides and well-crystallized iron oxides) present a decreasing trend with increasing distance from Liwu dam. Zn in sediments is mainly associated with easily-reducible Fe–Mn oxide, with proportions of 29.3–68.7%.

5. Discussion

5.1. Identification of Zn sources in paddy soils

The δ^{66}Zn values of paddy soils show a significant negative correlation with the EF_{Zn} (Fig. 4), indicating the Zn isotope signatures of pollution sources may be well preserved in paddy soils. To identify the sources of Zn, a mixing relationship based on the Zn concentrations and isotope compositions is considered here. Similar to several previous studies (e.g. Chen et al., 2008; Araújo et al., 2017), in a plot between 1/Zn (i.e. inverse concentration) and δ^{66}Zn value, any line shall define a binary mixing relationship. Fig. 5 shows that the paddy soil (TS-0) irrigated by the unpolluted TP river can be explained by the mixing of fertilizer and bedrock whereas the paddy soil from the mining-affected HS river irrigation area, falls on the mixing line between AMD-precipitate and fertilizer.

These results suggest that the δ^{66}Zn values of samples around the Dabaoshan mine are mainly controlled by three sources: bedrock, agricultural activities (i.e. fertilizer), and mining wastes (i.e. AMD-precipitate). Because weathering and pedogenesis of parent materials only lead to a marginal Zn isotope fractionation (Imseng et al., 2019; Vance et al., 2016), the δ^{66}Zn value of parent material remnant in soils can be represented by the bedrock. Moreover, anthropogenic inputs (i.e. including fertilizer and AMD-precipitate) might have overprinted δ^{66}Zn values of the parent material in the mining-affected paddy soils, which is consistent with previous studies (Imseng et al., 2019).

In addition, dry depositions have been suggested as the main pollution source with light Zn isotope composition in many previous studies (Mattielli et al., 2009; Bigalke et al., 2010; Juillot et al., 2011; Xia et al., 2020). However, dry depositions are not considered in the study area due to the following three reasons. First, the paddy field cannot be considered a downwind receptor for the mining area according to the predominant wind directions (Fig. 1). Second,

Table 2
Zn isotope compositions, metal concentrations and other relevant parameters in the environmental media.

Site	Sample	δ^{66}Zn (‰)	2SD[a]	pH	Fe (g kg^{-1})	Zn (mg kg^{-1})
AMD-precipitate						
1	DC-1	−0.14	0.03	4.16	120	1000
1	DC-1′	−0.12	0.04	4.10	151	710
2	DC-2	−0.22	0.07	2.55	127	1030
3	DC-3	−0.28	0.04	4.07	158	730
3	DC-3′	−0.31	0.04	4.05	153	960
3	DC-3″	−0.28	0.05	4.18	139	670
Sulfide ore						
	DK-1	0.15	0.06	–	361	770
	DK-2	0.11	0.00	–	322	220
	DK-3	0.04	0.03	–	515	710
Dry deposition						
	Y1	−0.26	0.00	–	2.89	157
	Y2	−0.18	0.04	–	3.83	74
	Y3	−0.18	0.01	–	2.60	314
Fertilizer						
	DF	0.11	0.05	–	2.25	150
Bulk rice plant[b]						
	Rice 1	−0.24	0.01	–	–	–
	Rice 2	−0.17	0.02	–	–	–
Parent material						
	Bedrock	0.01	0.03	–	32.6	14.2
	Bedrock 2	−0.01	0.02	–	35.3	12.4
HS river Sediment						
5	DC-5	−0.16	0.00	6.14	118	1020
8	DC-8	−0.03	0.01	8.15	97	3130
11	DC-11	−0.12	0.03	7.07	112	4000
14	DC-14	−0.03	0.03	7.25	34.4	570
TP river Sediment						
10	TC-10	0.13	0.05	7.64	28.8	102
Reference material						
	GSP-2	0.86	0.03	–	–	–
	NOD-A-1	0.75	0.04	–	–	–
	BHVO-2	0.08	0.02	–	–	–
Site	Sample	δ^{66}Zn (‰)	2SD[a]	pH	Fe (mg L^{-1})	Zn (mg L^{-1})
AMD						
1	DW-1	−0.02	0.04	2.41	395	132
1	DW-1′	0.01	0.04	2.45	348	118
3	DW-3	−0.04	0.07	2.41	350	117
3	DW-3′	0.04	0.05	2.44	374	125
HS River water						
5	DW-5	0.05	0.06	6.43	2.84	2.89
6	DW-6	0.08	0.06	6.57	2.60	2.15
7	DW-7	−0.03	0.01	6.78	1.48	0.19
8	DW-8	0.14	0.07	6.86	1.80	1.02
11	DW-11	0.15	0.04	6.93	1.29	1.18
12	DW-12	0.08	0.07	7.36	2.28	0.067
14	DW-14	0.28	0.01	8.11	0.71	0.10
TP River water						
10	TW-0	−0.02	0.01	7.84	0.16	0.0066
Rain water						
	Rain	−0.14	0.02	7.12	–	0.012
	Rain 2	−0.07	0.05	7.03	–	0.025

[a] 2 times the standard deviation of δ^{66}Zn was calculated from the replicates of each sample.
[b] The δ^{66}Zn of bulk rice plant was calculated based on equation (3). The δ^{66}Zn values in different organs of rice plants are shown in Table S2.

the Zn deposition flux in the study area (27.27 mg/m^2/yr) is much less than the average Zn deposition flux in China (108.75 ± 95.49 mg/m^2/yr) (Peng et al., 2019). Third, the TS-0 collected near the DS-11 shows an obviously different Zn concentration and Zn isotope composition from DS-11 (Table 1), which is inconsistent with the feature caused by the dry deposition input. Another potential Zn source for agriculture has been suggested to be pig slurry (Fekiacova et al., 2015; Imseng et al., 2019). However, the pig slurry is not widely used in this area, indicating the contribution from pig slurry to the paddy soils is expected to be limited.

To further quantify the contribution of mining and agricultural activities to the paddy soils in HS river irrigation area, the binary mixing equations in mass-balance are used as follows:

$$\delta^{66}Zn_{sample} = f_{mining}\delta^{66}Zn_{mining} + f_{agricultural}\delta^{66}Zn_{agricultural} \quad (4)$$

$$1 = f_{mining} + f_{agricultural} \quad (5)$$

where $\delta^{66}Zn_{sample}$, $\delta^{66}Zn_{mining}$, and $\delta^{66}Zn_{agricultural}$ are δ^{66}Zn values of the paddy soil samples, mining end-member, and agricultural end-member, respectively. f_{mining} and $f_{agricultural}$ are proportions of the two end-members. The average δ^{66}Zn value (−0.29 ± 0.03‰) of the AMD-precipitate samples (DC-3, DC-3′, and DC-3″) from site 3 is used as the characteristic δ^{66}Zn value of mining end-member, given that these samples were collected from the outlet of Liwu tailings dam and thus are highly representative of mining end-member. The δ^{66}Zn value of fertilizer (δ^{66}Zn = 0.11 ± 0.05‰) is adopted as the characteristic δ^{66}Zn value of agricultural end-member.

The calculation results show that the mining end-member is the main source of Zn in the mining-affected paddy soils (average contribution of 66.2%), but the contribution has significant spatial variations. Fig. 6a shows the relative contributions of mining and agricultural inputs to the topsoils. The mining contributions to the topsoils from the upper reach of the HS river are obviously higher than those from the lower reach, suggesting that the mining activities have relatively low impacts on the lower reach. The contributions of mining activities for soil profiles are shown in Fig. 6b and c. In TX profile, the mining activity is the main contributor along the whole profile, with an average contribution of ~85.0%, indicating that Zn from the mining activities has reached the deep soils in the upper reach irrigation area of the HS river. In SL profile, the soil profile located in lower reach of the HS river, the high contribution of mining activities is only observed in the surface horizon (A horizon), implying that the contributions of mining activities are limited in the deep soils in the lower reach irrigation area.

5.2. Zinc migration processes in the mining-affected region

5.2.1. The form of Zn in the mining end-member

Fig. 5 suggests that some precipitates from (AMD) can serve as the mining end-member contributing to the Zn pollution in paddy soils along the HS river. In the Liwu tailings dam, the δ^{66}Zn values of AMD-precipitates (−0.31 to −0.12‰) are lower than those of both sulfide ores (0.04 to 0.15‰) and AMD (−0.04 to 0.04‰). Interestingly, the apparent Zn isotope fractionation factor between AMD and sulfide ore ($\Delta^{66}Zn_{\text{AMD-sulfide ore}}$ = −0.19 to 0‰) observed in this study is similar to that between leachate and the sulfide-rich rocks ($\Delta^{66}Zn_{\text{solution-rock}}$ value of −0.20 to 0‰) determined in leaching experiments (Fernandez and Borrok, 2009), implying that Zn in the AMD is mostly derived from the oxidation and elution through sulfide ore. Moreover, compared with the AMD samples, the AMD-precipitates are enriched in ^{64}Zn with the Zn isotope fractionation factor between precipitates and AMD ($\Delta^{66}Zn_{\text{AMD-precipitate – AMD}}$) of −0.35 to −0.08‰, which agrees with the results of precipitation experiments (Archer et al., 2004), indicating AMD-precipitates uptake Zn from AMD. The integrated effects of the elution and precipitation processes lead to a significant enrichment of ^{64}Zn in AMD-precipitates compared with ores ($\Delta^{66}Zn_{\text{AMD-precipitate-sulfide ore}}$ = −0.46 to −0.16‰).

As a complex mixture, the AMD-precipitate is normally enriched in co-precipitated secondary minerals, including jarosite, goethite,

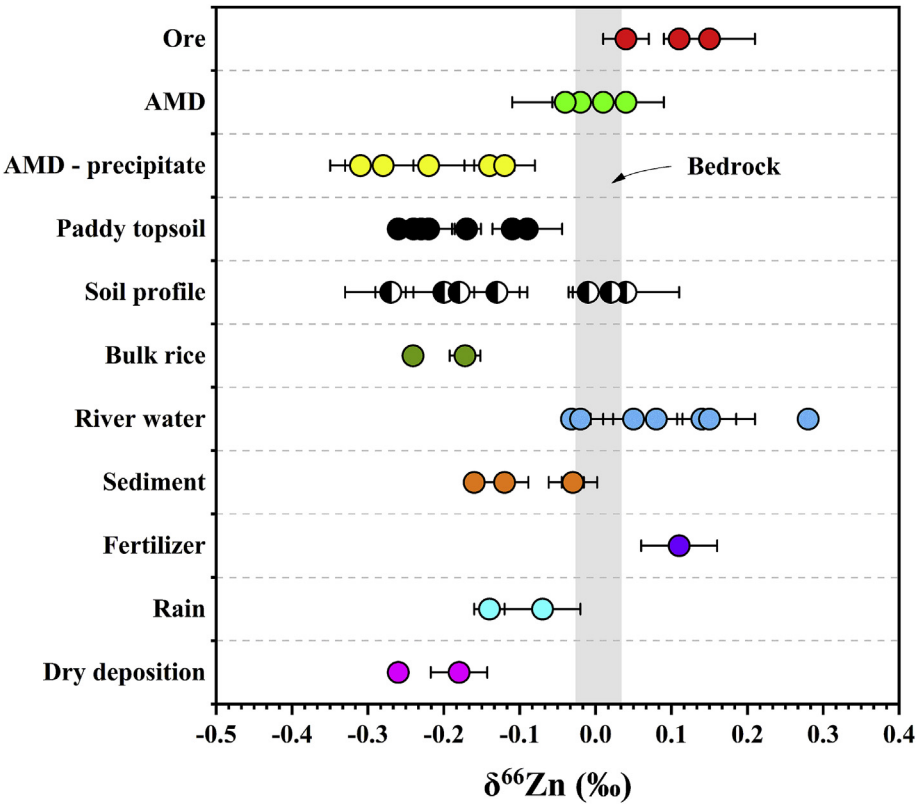

Fig. 2. δ^{66}Zn values in different environmental samples.

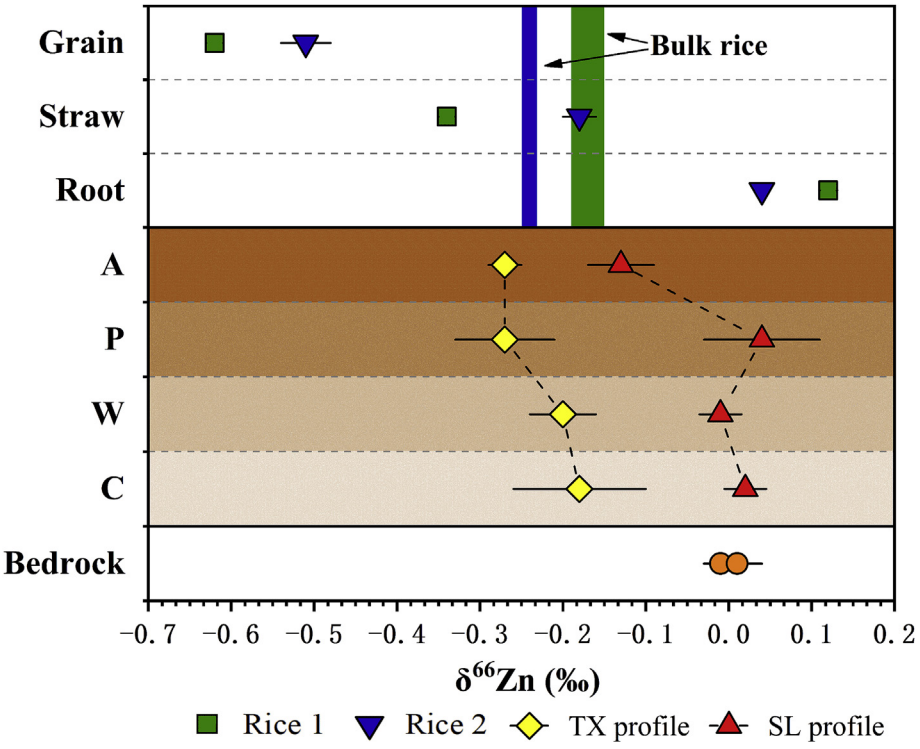

Fig. 3. Zn isotope compositions of soil profiles, bedrock and rice plants.

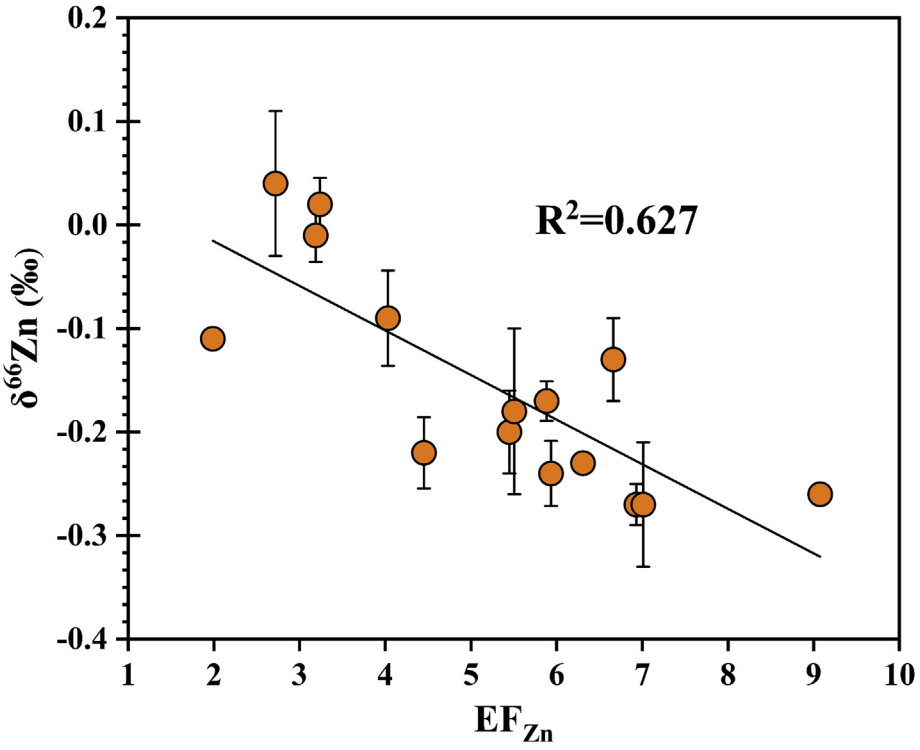

Fig. 4. $\delta^{66}Zn$ values versus EF_{Zn} for paddy soils (include topsoils and soil profiles).

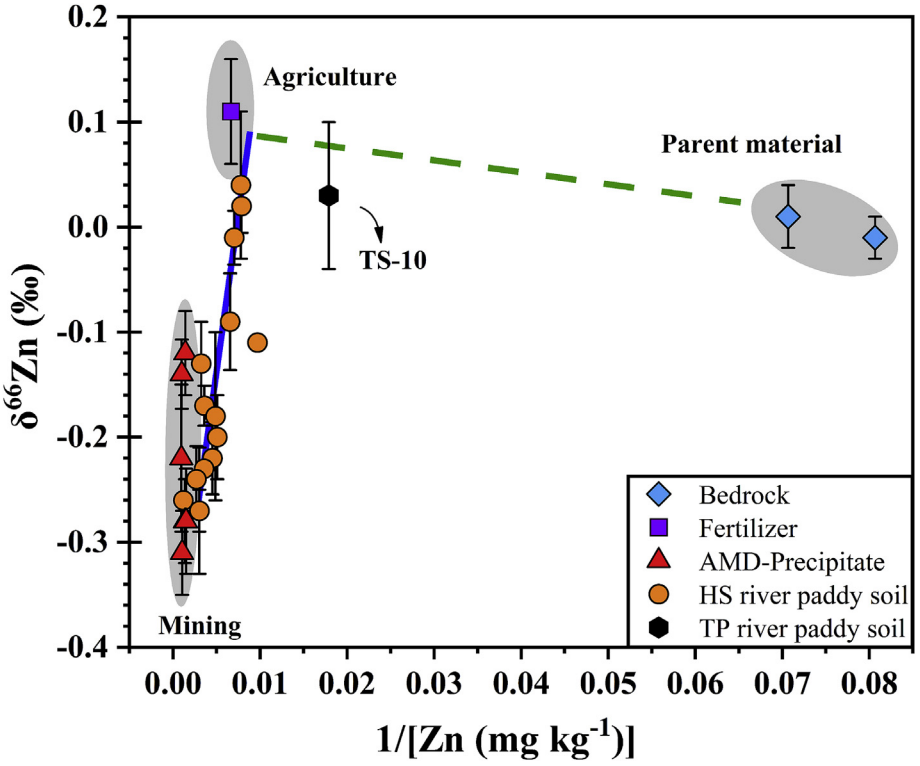

Fig. 5. $\delta^{66}Zn$ values versus 1/Zn for paddy soils (include topsoils and soil profiles). The bedrock, fertilizer, and AMD-precipitate represent parent material, agricultural end-member, and mining end-member, respectively. The blue solid line represents the mixing line of mining and agriculture end-member in the HS river paddy soils. The green dotted line represents the mixing line of agriculture end-member and parent material in the TP river paddy soil. (For interpretation of the references to color in this figure legend, the reader is referred to the Web version of this article.)

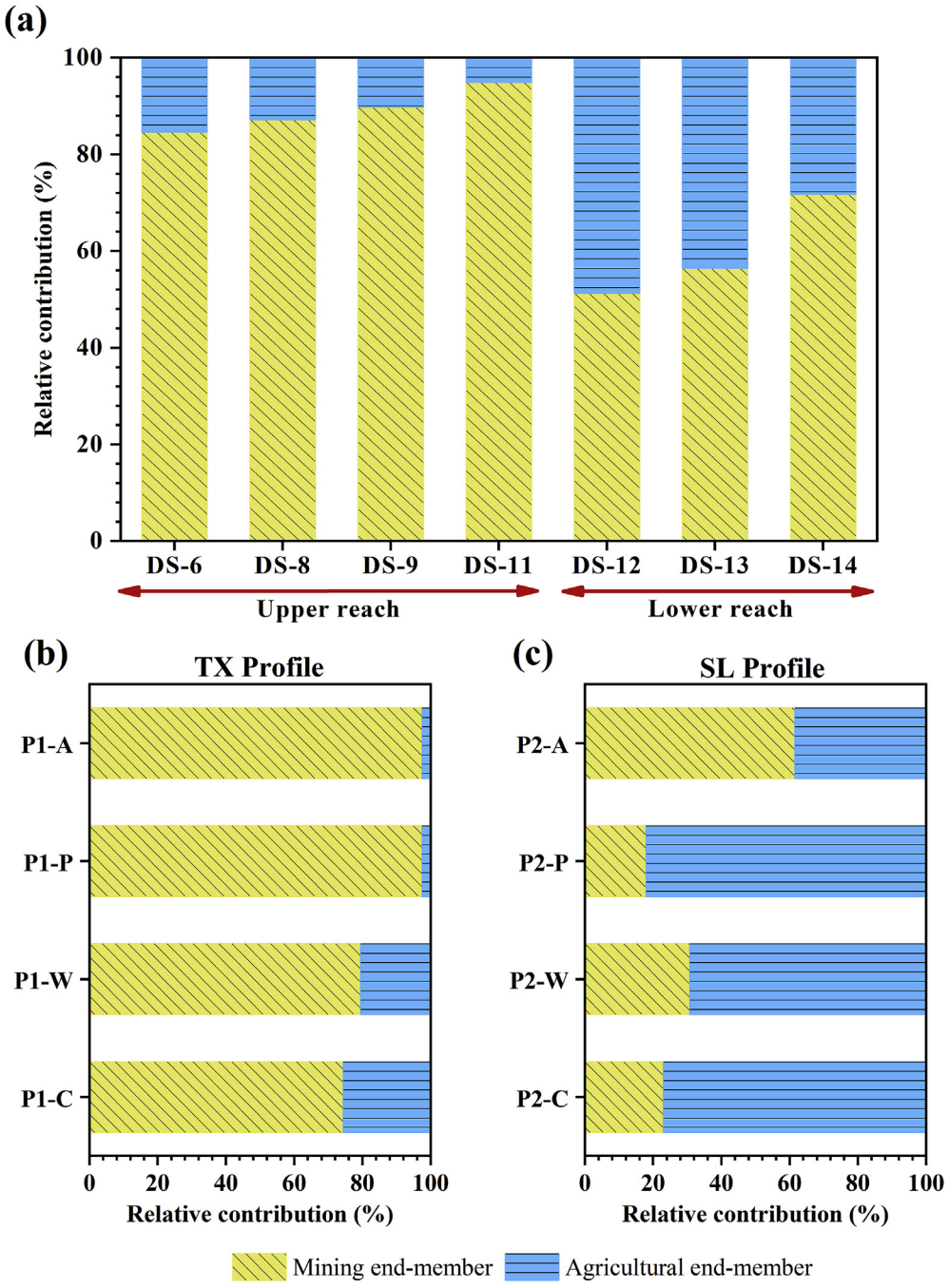

Fig. 6. Relative concentrations of mining and agricultural end-member for the paddy topsoil (a), TX soil profile (b), and SL soil profile (c).

schwertmannite, hematite and other Fe-bearing minerals (Liu et al., 2018). Because the AMD is the sulfuric acid-rich solution with pH < 2.5, the adsorption effect is limited in the tailings dam for Zn. For example, goethite is one of the potential adsorbents in the AMD-precipitate samples and the ratio of adsorbed Zn on goethite was reported to be only 1% at pH = 4 (Juillot et al., 2008). Because Zn minerals are not detected and Fe-bearing minerals are the main secondary minerals in the AMD-precipitates (Table S3), the dissolved Zn in the AMD may migrate into the AMD-precipitates through coprecipitation with the Fe-bearing secondary minerals (i.e. jarosite and goethite), as observed in Chen et al. (2015).

After being discharged from the tailings dam, the AMD-precipitates transport and deposit along with river water of the HS river. However, jarosite is ritually disappeared in the river sediments from the upper reach but the Fe and Zn concentrations are not less than the AMD-precipitates (Table 2). This can be understood if jarosite transforms to more crystalline secondary Fe(III) minerals (Karimian et al., 2017). For example, the Fe-sulfate may transform to the iron oxide (e.g. goethite) during the migration in the river system, in which some Zn is upheld in the mineral phase. The AMD-precipitates can further enter into the soil system from the HS river and act as the main source for the Zn pollution, which lead the Fe-oxide minerals to be the main carriers of Zn in the paddy soils (Fig. S1).

In contrast, the AMD-precipitates have a limited effect on the lower reach of the HS river, which can be explained by the dilution

effect. Compared to the sediments from upper reach, the sediments from the lower reach of the HS river contain less goethite and lower Zn concentrations (Table 2 and Table S3). This change occurs prominently after the confluence of the HS and TP rivers. Yang et al. (2019) reported that the Cd concentrations in the HS river water were diluted at the lower reach. Considering such a low Zn concentration (~102 mg kg^{-1}) and goethite content (~2.9%) in the TP river sediment (TC-10), the content of AMD-precipitates in the lower reach of the HS river system may also be diluted by the TP river, which further lead to the difference between the contributions of mining activities in the topsoils from the upper reach and the lower reach of HS river (Fig. 6a).

5.2.2. Loss of Zn from paddy soils

Zn in paddy soils can be removed due to the uptake by plants and surface run-off back to the river. However, our study shows that Zn uptake by plants makes limited modification to the δ^{66}Zn values of paddy soils for the following two reasons. First, although the mining-affected paddy soils have higher concentrations of Zn than others, the low Zn fraction in the exchangeable phase (1.8−14.6%) (Fig. S1) significantly limits the amount of Zn to be effectively used by plants. Second, even though the δ^{66}Zn values in various parts of rice plant show significant and systematic differences, the mass balance calculation shows that the Zn isotope compositions of bulk rice are similar to those of the topsoils (Fig. 2). Thus, the apparent Zn isotope fractionation between the bulk rice plants and paddy soils can be very limited ($\Delta^{66}Zn_{plant\text{-}soil} = -0.04$ to 0.02‰).

In contrast, the surface run-off might have led systematic variations in δ^{66}Zn values of paddy topsoils. As shown in Fig. 7, the δ^{66}Zn values of paddy topsoils along the upper or lower reach of HS river decrease but those of river water increase with increasing distance from Liwu dam. These systematic variations suggest a continuous removal of Zn from the topsoil to the river system. Imseng et al. (2019) reported that pH is the key factor controlling the Zn isotope fractionation in soil, and isotopically heavy Zn can be leached out of acidic soil. Moreover, Suhr et al. (2018) suggested that the δ^{66}Zn values of river water tend to increase in (sub)tropical region which may be controlled by the oxide-rich soil. The topsoils in this study are slightly acidic (pH = 5.58 to 6.51) (Table 1) and contain relatively high abundance of Fe-oxide minerals (Table S3), the heavy Zn isotopes associated with Fe-oxide minerals in these mining-affected paddy soils may have be exported to the river system. Therefore, the polluted soil may be an important source of Zn in the river water.

6. Conclusions and implications

Mining-affected soils often suffer from the heavy metal pollution and further threaten the human health. To solve this environment issue fundamentally, tracing the sources and migration processes of heavy metals in soils are critical. Based on the Zn isotopes, our study shows that mining end-member (i.e. AMD-precipitate) contributed the most of Zn in the mining-effected paddy soils (average contribution of 66.2%) and the agriculture end-member (i.e. fertilizer) placed second. These two sources even overprint the natural Zn in the paddy soils. Moreover, the contribution of mining activities in paddy soils has significant spatial variations within the mining-affected region. Specifically, the mining activities have relatively low impacts on the lower reach and the deep soil. Our findings also demonstrate that the dissolved Zn in the AMD may migrate into the AMD-precipitates by coprecipitation with the Fe-bearing secondary minerals (i.e. jarosite and goethite) and further enter into the river system and soil system. In these processes, Fe-bearing minerals are the main Zn carriers within the mining-affected region.

Our study highlights the contribution of both mining and

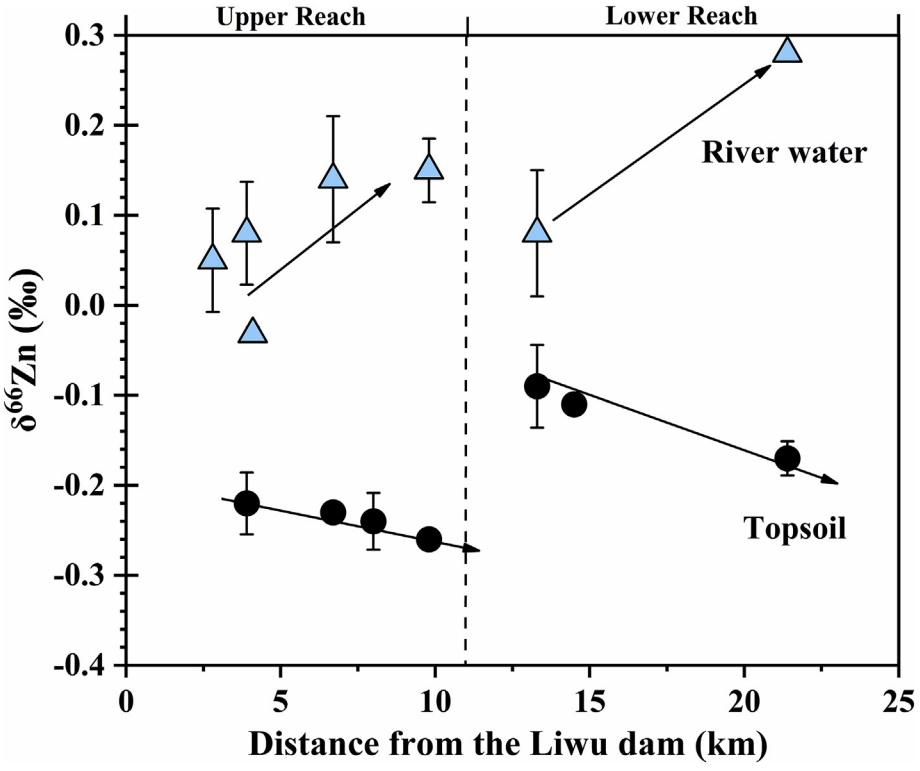

Fig. 7. δ^{66}Zn values of paddy topsoils and river water along HS river from Liwu tailings dam. The black dots and blue triangles represent topsoils and river water, respectively. (For interpretation of the references to color in this figure legend, the reader is referred to the Web version of this article.)

agricultural activities to the Zn pollution in the paddy soils. These findings provide an important scientific basis for developing a reasonable and economical pollution control policy for the mining-affected soil. Our study also highlights the important role of Fe-bearing minerals in Zn migration, which tells that more attention should be paid to control the release of Zn in the secondary iron oxides during the contamination control processes. Furthermore, our results demonstrate the Zn isotope is a powerful indicator of heavy metal pollution in a complex mining-affected area.

Authorship Contribution Statement

Yuhui Liu, Investigation, Data curation, Writing - original draft. Ting Gao, Conceptualization, Writing - review & editing. Yafei Xia, Investigation, Methodology. Zhengrong Wang, Formal analysis. Chengshuai Liu, Supervision. Shehong Li, Resources. Qiqi Wu, Project administration. Meng Qi, Project administration. Yiwen Lv, Funding acquisition.

Declaration of competing interest

The authors declare that they have no known competing financial interests or personal relationships that could have appeared to influence the work reported in this paper.

Acknowledgments

We thank Dr. Yang Tang for help in the MC-ICPMS lab. This work was financially supported by the National Natural Science Foundation of China (U1701241 and 41701266), the Key Scientific Research Projects of the Chinese Academy of Sciences (QYZDB-SSW-DQC046), the GDAS' Project of Science and Technology Development (2019GDASYL-0104016 and 2019GDASYL-0103048), the Science and Technology Planning Project of Guangdong Province, China (2017BT01Z176 and 2019B121205006), and the Construction Project of Modern Agricultural Science and Technology Innovation Alliance of Guangdong Province, China (2016LM2149).

Appendix A. Supplementary data

Supplementary data to this article can be found online at https://doi.org/10.1016/j.envpol.2020.115616.

References

Acosta, J.A., Faz, A., Martínez-Martínez, S., Zornoza, R., Carmona, D.M., Kabas, S., 2011. Multivariate statistical and GIS-based approach to evaluate heavy metals behavior in mine sites for future reclamation. J. Geochem. Explor. 109, 8–17.

Araújo, D.F., Boaventura, G.R., Machado, W., Viers, J., Weiss, D., Patchineelam, S.R., Ruiz, I., Rodrigues, A.P.C., Babinski, M., Dantas, E., 2017. Tracing of anthropogenic zinc sources in coastal environments using stable isotope composition. Chem. Geol. 449, 226–235.

Archer, C., Vance, D., Butler, I., 2004. Abiotic Zn isotope fractionations associated with ZnS precipitation. Geochem. Cosmochim. Acta 68 (11). Supplement 325.

Arnold, T., Kirk, G.J., Wissuwa, M., Frei, M., Zhao, F.J., Mason, T.F., Weiss, D.J., 2010. Evidence for the mechanisms of zinc uptake by rice using isotope fractionation. Plant Cell Environ. 33, 370–381.

Bigalke, M., Weyer, S., Kobza, J., Wilcke, W., 2010. Stable Cu and Zn isotope ratios as tracers of sources and transport of Cu and Zn in contaminated soil. Geochem. Cosmochim. Acta 74, 6801–6813.

Bryan, A.L., Dong, S., Wilkes, E.B., Wasylenki, L.E., 2015. Zinc isotope fractionation during adsorption onto Mn oxyhydroxide at low and high ionic strength. Geochem. Cosmochim. Acta 157, 182–197.

China Environmental Monitoring Station, 1990. Natural Background Values of Soil Elements in China. China Environmental Science Press, Beijing (in Chinese).

Chen, H., Savage, P.S., Teng, F.Z., Helz, R.T., Moynier, F., 2013. Zinc isotope fractionation during magmatic differentiation and the isotope composition of the bulk Earth. Earth Planet Sci. Lett. 369–370, 34–42.

Chen, J., Gaillardet, J., Louvat, P., 2008. Zinc isotopes in the Seine River waters, France: a probe of anthropogenic contamination. Environ. Sci. Technol. 42 (17), 6494–6501.

Chen, J., Gaillardet, J., Louvat, P., Huon, S., 2009. Zn isotopes in the suspended load of the Seine River, France: isotope variations and source determination. Geochem. Cosmochim. Acta 73, 4060–4076.

Chen, M.Q., Lu, G.N., Guo, C.L., Yang, C., Wu, J., Huang, W.L., 2015. Sulfate migration in a river affected by acid mine drainage from the Dabaoshan mining area, South China. Chemosphere 119, 734–743.

Chen, M.Q., Lu, G.N., Wu, J.X., Yang, C.F., Niu, X.C., Tao, X.Q., Shi, Z.Q., Yi, X.Y., Dang, Z., 2018. Migration and fate of metallic elements in a waste mud impoundment and affected river downstream: a case study in Dabaoshan Mine, South China. Ecotoxicol. Environ. Saf. 164, 474–483.

Chen, S., Liu, Y., Hu, J., Zhang, Z., Hou, Z., Huang, F., Yu, H., 2016. Zinc isotope compositions of NIST SRM 683 and whole-rock reference materials. Geostand. Geoanal. Res. 40 (3), 417–432.

Cheng, H., Hu, Y., 2010. Lead (Pb) isotopic fingerprinting and its applications in lead pollution studies in China: a review. Environ. Pollut. 158, 1134–1146.

Dold, B., 2014. Evolution of acid mine drainage formation in sulphidic mine tailings. Minerals 4, 621–641.

Fekiacova, Z., Cornu, S., Pichat, S., 2015. Tracing contamination sources in soils with Cu and Zn isotope ratios. Sci. Total Environ. 517, 96–105.

Fernandez, A., Borrok, D.M., 2009. Fractionation of Cu, Fe, and Zn isotopes during the oxidative weathering of sulfide-rich rocks. Chem. Geol. 264, 1–12.

Gao, T., Ke, S., Wang, S.-J., Li, F., Liu, C., Lei, J., Liao, C., Wu, F., 2018. Contrasting Mg isotopic compositions between Fe-Mn nodules and surrounding soils: accumulation of light Mg isotopes by Mg-depleted clay minerals and Fe oxides. Geochem. Cosmochim. Acta 237, 205–222.

Gou, W., Li, W., Ji, J., Li, W., 2018. Zn isotope fractionation during sorption on Al oxide: atomic level understanding from EXAFS. Environ. Sci. Technol. 52, 9087–9096.

Guinoiseau, D., Gélabert, A., Moureau, J., Louvat, P., Benedetti, M.F., 2016. Zn isotope fractionation during sorption onto kaolinite. Environ. Sci. Technol. 50, 1844–1852.

Imseng, M., Wiggenhauser, M., Müller, M., Keller, A., Frossard, E., Wilcke, W., Bigalke, M., 2019. The fate of Zn in agricultural soils: a stable isotope approach to anthropogenic impact, soil formation, and soil–plant cycling. Environ. Sci. Technol. 53, 4140–4149.

Jouvin, D., Louvat, P., Juillot, F., Marechal, C., Benedetti, M., 2009. Zinc isotope fractionation: why organic matters? Environ. Sci. Technol. 43, 5747–5754.

Juillot, F., Maréchal, C., Ponthieu, M., Cacaly, S., Morin, G., Benedetti, M., Hazemann, J.L., Proux, O., Guyot, F., 2008. Zn isotope fractionation caused by sorption on goethite and 2-Lines ferrihydrite. Geochem. Cosmochim. Acta 72, 4886–4900.

Juillot, F., Maréchal, C., Morin, G., Jouvin, D., Sylvain, C., Telouk, P., Benedetti, M.F., Ildefonse, P., Sutton, S., Guyot, F., Brown, J.G.E., 2011. Contrasting isotope signatures between anthropogenic and geogenic Zn and evidence for post-depositional fractionation processes in smelter-impacted soils from northern France. Geochem. Cosmochim. Acta 75, 2295–2308.

Karimian, N., Johnston, S.G., Burton, E.D., 2017. Antimony and arsenic behavior during Fe (II)-induced transformation of Jarosite. Environ. Sci. Technol. 51, 4259–4268.

Kumar, M., Furumai, H., Kasuga, I., Kurishu, F., 2020. Metal partitioning and leaching vulnerability in soil, soakaway sediments, and road dust in the urban area of Japan. Chemosphere 252, 126605.

Kumar, M., Furumai, H., Kurishu, F., Kasuga, I., 2009. Understanding the partitioning processes of mobile lead in soakaway sediments using sequential extraction and isotope analysis. Water Sci. Technol. 60 (8), 2085–2091.

Li, W., Gou, W., Li, W., Zhang, T., Yu, B., Liu, Q., Shi, J., 2019. Environmental applications of metal stable isotopes: Silver, mercury and zinc. Environ. Pollut. 252B, 1344–1356.

Li, Z., Ma, Z., van der Kuijp, T.J., Yuan, Z., Huang, L., 2014. A review of soil heavy metal pollution from mines in China: pollution and health risk assessment. Sci. Total Environ. 468–469, 843–853.

Liu, H.G., Probsta, A., Liao, B.H., 2005. Metal contamination of soils and crops affected by the Chenzhou lead/zinc mine spill (Hunan, China). Sci. Total Environ. 339, 153–166.

Liu, J., Yin, M., Zhang, W., Tsang, D., Wei, X., Zhou, Y., Xiao, T., Wang, J., Dong, X., Sun, Y., Chen, Y., Li, H., Hou, L., 2019. Response of microbial communities and interactions to thallium in contaminated sediments near a pyrite mining area. Environ. Pollut. 248, 916–928.

Liu, Q., Chen, B., Haderlein, S., Gopalakrishnan, G., Zhou, Y.Z., 2018. Characteristics and environmental response of secondary minerals in AMD from Dabaoshan Mine, South China. Ecotoxiol. Environ. Saf. 155, 50–58.

Lv, Y., Liu, S.A., Zhu, J.M., Li, S., 2016. Copper and zinc isotope fractionation during deposition and weathering of highly metalliferous black shales in central China. Chem. Geol. 422, 24–35.

Mavromatis, V., Gonzalez, A.G., Dietzel, M., Schott, J., 2019. Zinc isotope fractionation during the inorganic precipitation of calcite – towards a new pH proxy. Geochem. Cosmochim. Acta 244, 99–112.

Mattielli, N., Petit, J.C.J., Deboudt, K., Flament, P., Perdrix, E., Taillez, A., Rimetz-Planchon, J., Weis, D., 2009. Zn isotope study of atmospheric emissions and dry depositions within a 5 km radius of a Pb–Zn refinery. Atmos. Environ. 43, 1265–1272.

Moeller, K., Schoenberg, R., Pedersen, R.B., Weiss, D., Dong, S., 2012. Calibration of the New Certified Reference Materials ERM-AE633 and ERM-AE647 for copper and IRMM-3702 for zinc isotope amount ratio determinations. Geostand. Geoanal. Res. 36 (2), 177–199.

Moynier, F., Vance, D., Fujii, T., Savage, P., 2017. The isotope geochemistry of zinc and copper. Rev. Mineral. Geochem. 82, 543–600.
Peng, H., Chen, Y.L., Weng, L.P., Ma, J., Ma, Y.L., Li, Y.T., Islam, M.S., 2019. Comparisons of heavy metal input inventory in agricultural soils in North and South China: a review. Sci. Total Environ. 660, 776–786.
Perl, J., Shin, J., Schümann, J., Faddegon, B., Paganetti, H., 2012. TOPAS: an innovative proton Monte Carlo platform for research and clinical applications. Med. Phys. 39 (11), 6818–6837.
Pokrovsky, O.S., Viers, J., Freydier, R., 2005. Zinc stable isotope fractionation during its adsorption on oxides and hydroxides. J. Colloid Interface Sci. 291, 192–200.
Qu, L., Xie, Y.Y., Lu, G., Yang, C.F., Zhou, J.N., Yi, X.Y., Dang, Z., 2017. Distribution, fractionation, and contamination assessment of heavy metals in paddy soil related to acid mine drainage. Paddy Water Environ. 15, 553–562.
Roebbert, Y., Rabe, K., Lazarov, M., Schuth, S., Schippers, A., Dold, B., Weyer, S., 2018. Fractionation of fe and cu isotopes in acid mine tailings: modification and application of a sequential extraction method. Chem. Geol. 493, 67–79.
Schudel, G., Miserendino, R.A., Veiga, M.M., Velasquez-López, P.C., Lees, P.S.J., Winland-Gaetz, S., Davée Guimarães, J.R., Bergquist, B.A., 2018. An investigation of mercury sources in the Puyango-Tumbes River: using stable Hg isotopes to characterize transboundary Hg pollution. Chemosphere 202, 777–787.
Sherman, L.S., Blum, J.D., Dvonch, J.T., Gratz, L.E., Landis, M.S., 2015. The use of Pb, Sr, and Hg isotopes in Great Lakes precipitation as a tool for pollution source attribution. Sci. Total Environ. 502, 362–374.
Shiel, A.E., Weis, D., Orians, K.J., 2010. Evaluation of zinc, cadmium and lead isotope fractionation during smelting and refining. Sci. Total Environ. 408, 2357–2368.
Suhr, N., Schoenberg, R., Chew, D., Rosca, C., Widdowson, M., Kamber, B.S., 2018. Elemental and isotopic behaviour of Zn in Deccan basalt weathering profiles: chemical weathering from bedrock to laterite and links to Zn deficiency in tropical soils. Sci. Total Environ. 619–620, 1451–1463.
Vance, D., Matthews, A., Keech, A., Archer, C., Hudson, G., Pett-Ridge, J., Chadwick, O.A., 2016. The behaviour of Cu and Zn isotopes during soil development: controls on the dissolved load of rivers. Chem. Geol. 445, 36–53.
Weiss, D.J., Mason, T.F.D., Zhao, F.J., Kirk, G.J.D., Coles, B.J., Horstwood, M.S.A., 2005. Isotope discrimination of zinc in higher plants. New Phytol. 165, 703–710.
Wen, H.J., Zhang, Y.X., Cloquet, C., Zhu, C.W., Fan, H.F., Luo, C.G., 2015. Tracing sources of pollution in soils from the Jinding Pb–Zn mining. Appl. Geochem. 52, 147–154.
Wiederhold, J.G., 2015. Metal stable isotope signatures as tracers in environmental geochemistry. Environ. Sci. Technol. 49, 2606–2624.
Wiggenhauser, M., Bigalke, M., Imseng, M., Keller, A., Archer, C., Wilcke, W., Frossard, E., 2018. Zinc isotope fractionation during grain filling of wheat and a comparison of zinc and cadmium isotope ratios in identical soil-plant systems. New Phytol. 219, 195–205.
Wimpenny, J., Marks, N., Knight, K., Rolison, J.M., Borg, L., Eppich, G., Badro, J., Ryerson, F.J., Sanborn, M., Huyskens, M.H., Yin, Q., 2019. Experimental determination of Zn isotope fractionation during evaporative loss at extreme temperatures. Geochem. Cosmochim. Acta 259, 391–411.
Wuana, R.A., Okieimen, F.E., 2011. Heavy metals in contaminated soils: a review ofsources, chemistry, risks and best available strategies for remediation. ISRN Ecology 2011 1–20.
Xia, Y.F., Gao, T., Liu, Y.H., Wang, Z.R., Liu, C.S., Wu, Q.Q., Qi, M., Lv, Y.W., Li, F.B., 2020. Zinc isotope revealing zinc's sources and transport processes in karst region. Sci. Total Environ. 724, 138191.
Yang, W.J., Ding, K.B., Zhang, P., Qiu, H., Cloquet, C., Wen, H.J., Morel, J.L., Qiu, R.L., Tang, Y.T., 2019. Cadmium stable isotope variation in a mountain area impacted by acid mine drainage. Sci. Total Environ. 646, 696–703.
Ye, L., Liu, T.G., Yang, Y.L., Gao, W., Pan, Z.P., Bao, T., 2014. Petrogenesis of bismuth minerals in the Dabaoshan Pb-Zn polymetallic massive sulfide deposit, northern Guangdong Province, China. J. Asian Earth Sci. 82, 1–9.
Yin, H., Tan, N., Liu, C., Wang, J., Liang, X., Qu, M., Feng, X., Qiu, G., Tan, W., Liu, F., 2016. The associations of heavy metals with crystalline iron oxides in the polluted soils around the mining areas in Guangdong Province, China. Chemosphere 161, 181–189.
Young, R.A., 1993. The Rietveld Method. International Union of Crystallography Monographs on Crystallography. Oxford University Press, NYC, NY, USA.
Zhang, J., Liu, Y., 2018. Zinc isotope fractionation under vaporization processes and in aqueous solutions. Acta Geochim 37, 663–675.
Zhao, F.J., Ma, Y.B., Zhu, Y.G., Tang, Z., McGrath, S.P., 2015. Soil contamination in China: current status and mitigation strategies. Environ. Sci. Technol. 49, 750–759.
Zhou, J.M., Dang, Z., Cai, M.F., Liu, C.Q., 2007. Soil heavy metal pollution around the dabaoshan mine, Guangdong Province, China. Pedosphere 17, 588–594.
Zimmermann, T., Mohamed, A.F., Reese, A., Wieser, M.E., Kleeberg, U., Pröfrock, D., Irrgeher, J., 2020. Zinc isotopic variation of water and surface sediments from the German Elbe River. Sci. Total Environ. 707, 135219.